On the Conformation of Dimeric Acceptors and Their Polymer Solar Cells with Efficiency over 18 %

How to cite: Angew. Chem. Int. Ed. 2023, e202302888
doi.org/10.1002/anie.202302888

Solar Cells Hot Paper

On the Conformation of Dimeric Acceptors and Their Polymer Solar Cells with Efficiency over 18 %

Jingnan Wu[+], Zhaoheng Ling[+], Leandro R. Franco, Sang Young Jeong, Zewdneh Genene, Josué Mena, Si Chen, Cailing Chen, C. Moyses Araujo, Cleber F. N. Marchiori, Joost Kimpel, Xiaoming Chang, Furkan H. Isikgor, Qiaonan Chen, Hendrik Faber, Yu Han, Frédéric Laquai, Maojie Zhang, Han Young Woo, Donghong Yu, Thomas D. Anthopoulos,* and Ergang Wang**

Abstract: The determination of molecular conformations of oligomeric acceptors (OAs) and their impact on molecular packing are crucial for understanding the photovoltaic performance of their resulting polymer solar cells (PSCs) but have not been well studied yet. Herein, we synthesized two dimeric acceptor materials, DIBP3F-Se and DIBP3F-S, which bridged two segments of Y6-derivatives by selenophene and thiophene, respectively. Theoretical simulation and experimental 1D and 2D NMR spectroscopic studies prove that both dimers exhibit *O*-shaped conformations other than *S*- or *U*-shaped counter-ones. Notably, this *O*-shaped conformation is likely governed by a distinctive "conformational lock" mechanism, arising from the intensified intramolecular π–π interactions among their two terminal groups within the dimers. PSCs based on DIBP3F-Se deliver a maximum efficiency of 18.09 %, outperforming DIBP3F-S-based cells (16.11 %) and ranking among the highest efficiencies for OA-based PSCs. This work demonstrates a facile method to obtain OA conformations and highlights the potential of dimeric acceptors for high-performance PSCs.

Introduction

Solution-processed polymer solar cells (PSCs) based on blends of donor- and acceptor-type photoactive materials have advanced rapidly in recent years due to significant progress in materials development.[1] The majority of current research mainly focuses on the development of small molecule acceptors (SMAs)[2] and polymer acceptors (PAs),[3] which provide power conversion efficiencies (PCEs) of over 18 %. SMAs based on ITIC- and Y6-derivatives offer easily tailorable molecular structures with tunable absorption spectra, suitable energy levels, and enhanced charge-carrier mobility that leads to lower energy losses (E_{loss}).[4] However, SMA-based PSCs still suffer from device stability related to the fast molecular diffusions and strong crystallizability of SMAs within the bulk heterojunctions (BHJs).[5] On the other hand, PA-based PSCs (especially for polymerized SMA) have demonstrated enhanced morphological stability and mechanical flexibility (e.g.

[*] J. Wu,[+] Z. Genene, J. Mena, J. Kimpel, Q. Chen, Prof. E. Wang
Department of Chemistry and Chemical Engineering, Chalmers University of Technology
41296 Göteborg (Sweden)
E-mail: ergang@chalmers.se

J. Wu,[+] Prof. D. Yu
Department of Chemistry and Bioscience, Aalborg University
9220 Aalborg (Denmark)
E-mail: yu@bio.aau.dk

Z. Ling,[+] S. Chen, X. Chang, F. H. Isikgor, H. Faber, F. Laquai, Prof. T. D. Anthopoulos
King Abdullah University of Science and Technology (KAUST), KAUST Solar Center
Thuwal 23955 (Saudi Arabia)
E-mail: thomas.anthopoulos@kaust.edu.sa

L. R. Franco, Prof. C. M. Araujo, Prof. C. F. N. Marchiori
Department of Engineering and Physics, Karlstad University
65188 Karlstad (Sweden)

S. Y. Jeong, Prof. H. Y. Woo
Department of Chemistry, Korea University
Seoul 02841 (Republic of Korea)

C. Chen, Prof. Y. Han
Advanced Membranes and Porous Materials Center, Physical Sciences and Engineering Division, King Abdullah University of Science and Technology
Thuwal 23955-6900 (Saudi Arabia)

Prof. C. M. Araujo
Materials Theory Division, Department of Physics and Astronomy, Uppsala University
75120 Uppsala (Sweden)

Prof. M. Zhang
National Engineering Research Center for Colloidal Materials, School of Chemistry & Chemical Engineering, Shandong University
Jinan, Shandong, 250100 (China)

[+] These authors contributed equally to this work.

tensile properties) as compared to SMA-based counterparts due to their high entropy-elasticity caused by their entanglement.[6] In spite of these, batch-to-batch variations in these polymers result in poor reproducibility of the attainable device performance.[7] Moreover, the low miscibility between different polymers causes the phase-separated domain sizes in PA-based BHJs to be larger than those formed in SMA-based blends and ultimately limits their device performance.[4,8]

Very recently, oligomeric acceptors (OAs) synthesized by coupling SMA segments (Y-series) with/without linkage units have emerged as a new family of acceptor materials.[9] OAs combine the advantages of both SMAs and PAs, which in turn help to overcome the above-mentioned drawbacks. Despite their potential, only a handful of OAs have been investigated for application in PSCs. For example, dimeric OAs based on two Y6-analogues linked together showed a high absorption coefficient, enhanced electron mobility, and more favorable morphology when blended with a polymer donor (PD), yielding PSCs with PCE values of 15.05 %,[9a] 16.06 %[9b] and 18.19 %,[9c] respectively. It was also found that the dimeric-type OA-based devices have shown similar photo- and thermal-stability[9b–c] to those based on PA and higher than traditional SMA-based ones, which is associated with higher glass transition temperatures (T_gs) and slower diffusion kinetics of the dimers due to their enlarged molecular sizes. Although OA-based PSCs have potential advantages, the molecular conformations of OAs and their impact have not been well studied. OAs with extended conjugated structures can result in different molecular conformations due to rotatable C–C single bonds between the conjugated blocks (SMA segments) and linking units. Some conformations may feature a more twisted backbone (dihedral angles $>20°$),[9a,b,10] which leads to undesirable molecular packing and blend morphology. Therefore, it is important to determine the conformations of OAs and understand the factors that may influence these.[11] It has been previously reported that non-covalent intramolecular interactions among atoms such as H···F, O···S, H···O, and S···F could act as a "conformational lock"[12] and promote the planarity of polymer backbones.[10,13] However, it must be noted that these conformations have primarily relied on density functional theory (DFT) calculations, which are simply based on the optimization of molecular geometries to model their specific isomers. This means that the intrinsic conformations of the molecules are not experimentally determined and the actual effect of "conformational lock" remains unclear. Therefore, further investigations that address these aforementioned knowledge gaps are imperative for gaining a comprehensive understanding of OAs.

Herein, two dimeric-type acceptor materials were synthesized by bridging two Y-series SMA (BTIC-3F) segments with selenophene (Se, gives DIBP3F-Se) and thiophene (T, yields DIBP3F-S) as linkage units, respectively. The conformational characteristics of these dimeric acceptors were investigated through a combination of spectroscopic (proton nuclear magnetic resonance (^{1}H NMR), 2D NMR, and ^{19}F NMR) complemented with DFT simulations. Both theoretical simulations and experimental measurements consistently reveal that both OAs feature the same preferred molecular conformations, namely *O*-shaped conformations other than *S*- or *U*-shaped counterparts. Remarkably, the formation of this conformation is not governed by the typical non-covalent intramolecular interactions so-called "conformational lock" reported in previous studies.[12] Instead, it may originate from a unique driving force induced by the strong intramolecular π–π interactions among their two terminal IC (2-(3-oxo-2,3-dihydro-1H-inden-1-ylidene) malononitrile) groups. Furthermore, a comparative analysis of the photophysical-, electronic-properties, and PSC performance of the two OAs was conducted. Compared with DIBP3F-S, DIBP3F-Se exhibits a more coplanar and rigid backbone, enhanced light absorption, a slightly upshifted lowest unoccupied molecular orbital (LUMO) energy level, tighter π–π stacking, and a more ordered molecular arrangement. When blended with the state-of-the-art PD of PM6, DIBP3F-Se-based blends show substantially improved device performance with a maximum PCE of 18.09 % and a reduced E_{loss} of 0.509 eV. Such photovoltaic (PV) performance is significantly higher than the cells made with DIBP3F-S which yield a PCE of 16.11 %. Moreover, in combination with other efficient PDs like D18 and PTQ-10 (structures are shown in Figure S1), the resulting DIBP3F-Se-based PSCs maintained an efficiency level surpassing 17 %, indicating that the dimeric acceptor has good compatibility with other donor polymers for achieving high performance.

Results and Discussion

The chemical structures of DIBP3F-Se and DIBP3F-S are shown in Figure 1a, and the detailed synthesis routes are presented in Scheme S1 in Supporting Information. The asymmetric monomer BTIC-3FBr was synthesized by means of a Knoevenagel reaction via adding mono-bromofluorinated and di-fluorinated IC in sequence into BT-2CHO-BO with two aldehyde end groups. Then, the dimeric-type acceptors DIBP3F-Se and DIBP3F-S were prepared through a Stille-coupling reaction catalyzed by $Pd_2(dba)_3$ and P(o-Tol)$_3$ between BTIC-3FBr and the linking unit of 2,5-bis(trimethylstannyl)selenophene and 2,5-bis(trimethylstannyl)thiophene, respectively. The structures of the intermediate BTIC-3FBr and the two target molecules were confirmed by the experimental results from ^{1}H NMR, ^{13}C NMR, and Matrix-Assisted Laser Desorption/Ionization Time of Flight Mass Spectrometry (MALDI-TOF MS). Both acceptors possess good solubility in chloroform and chlorobenzene, enabling solution-processed device fabrication. A weight loss of 5 % was observed at high temperatures of ~320 °C detected by thermogravimetric analysis (TGA, Figure S2), indicating good thermal stability.

DFT calculations, at the B3LYP-D3BJ/6-311G(d,p) theory level, were carried out to study molecular geometry and energy levels of frontier molecular orbitals of the two OAs. As shown in Figure S3, there are three possible conformations for the dimers, namely *U*- (conformation *U*), *S*- (conformation *S*) and *O*-shape (conformation *O*) with no

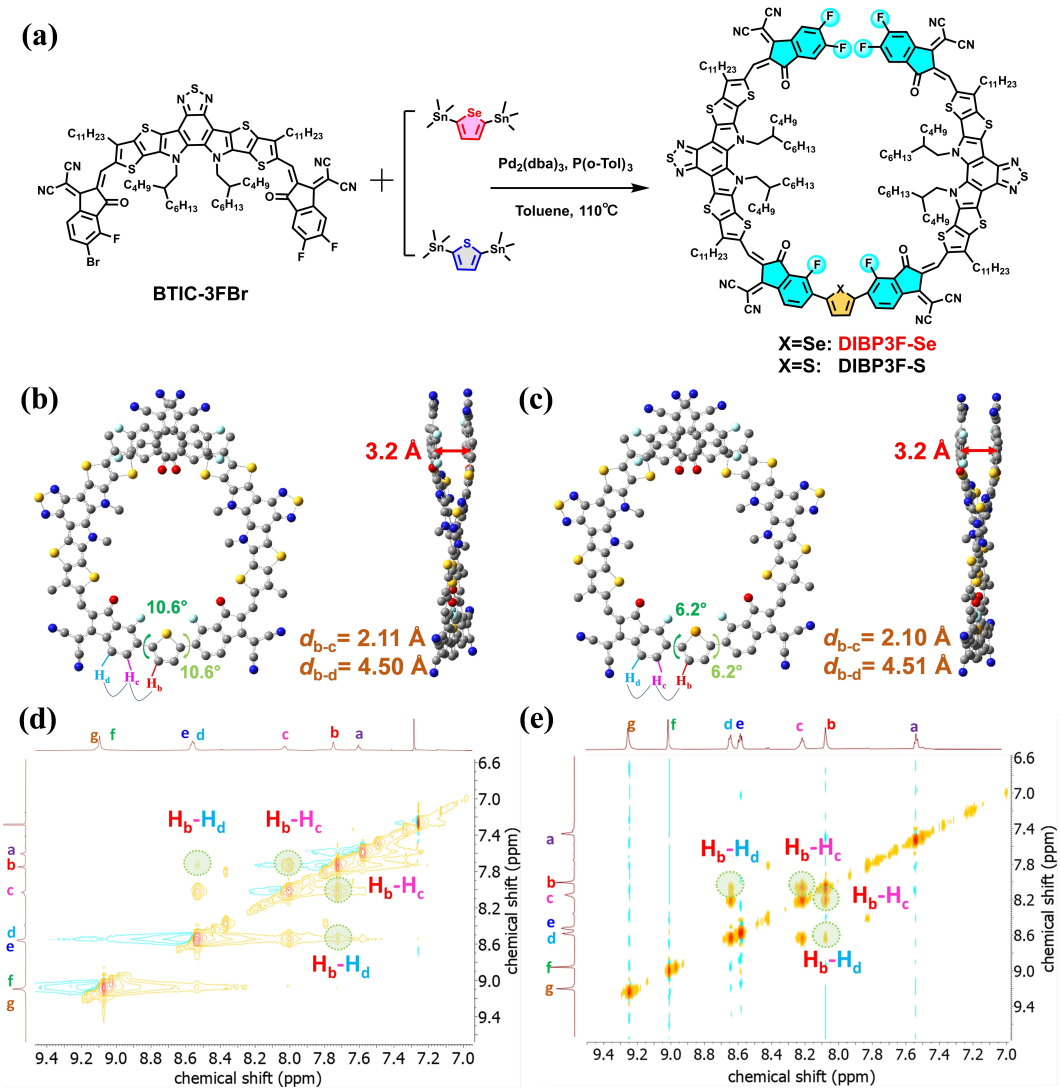

Figure 1. (a) The chemical structures and synthetic routes of DIBP3F-S and DIBP3F-Se. DFT-simulated molecular geometry from the top-view and side-view of the *O*-shaped molecular models for (b) DIBP3F-S and (c) DIBP3F-Se. (d) ^{1}H-^{1}H NMR spectrum (600 MHz) of DIBP3F-S in the $CDCl_3$ solution at 313 K. (e) ^{1}H-^{1}H NMR spectrum (700 MHz) of DIBP3F-Se in the CD_2Cl_4 solution at 333 K.

essential difference in energy levels. To identify the preferred conformation, the energetic stability was assessed by calculating the total Gibbs free energy, which encompasses the electronic energy, solvation energy, and thermal corrections. As shown in Table S1, the simulated results indicate that conformation *O* exhibits the highest stability (lowest free energy) for both DIBP3F-S and DIBP3F-Se compounds. Secondly, electron clouds′ distribution proven by the chemical shifts (δs) of ^{1}H in their NMR spectra would also strongly indicate their conformationally isomeric structures. The δ of the protons H_b and H_b' of both OAs with three different conformations in $CDCl_3$ solutions was modelled to compare with the experimental values.[14] Generally, the Se-based organic molecule presents higher δs for the protons on Se (H_b in Figure 1c) as compared to the corresponding T-based counterparts. The de-shielding of the Se-based protons is owing to the larger size and weaker electron affinity of selenium compared with that of the *S*-based ones.[15] As shown in Table S2, the simulated NMR δs for H_b show agreement with experimental ^{1}H NMR measurements (Figure S4–5) when considering conformation *O*. The absolute values of the δs, as well as the trend displaying an increase in δ from DIBP3F-S to DIBP3F-Se, are accurately reproduced by this conformation. In addition, the calculations for all other aromatic hydrogen atoms (from H_a to H_f) were also performed and a noteworthy agreement between experimental and theoretical values is observed for conformation *O*.

To further confirm the dimers' conformations, a detailed analysis of 2D NMR (^{1}H-^{1}H-Nuclear Overhauser Effect Spectroscopy (NOESY)) and ^{19}F NMR spectra were conducted. NOESY experiment affords a 2D δ correlation map similar in which through-space connectivities can be traced out, and the exchange cross-peaks will occur only when the protons are within a distance of 0.5 nm.[16] As shown in Figure S3, the inter-proton distances of H_b-H_c ($d_{b\text{-}c}$)/H_b-H_d

($d_{b\text{-}d}$) are estimated to be ~2.10/4.51, ~2.09/4.51 and ~4.75/6.29 Å for *O-, S-*, and *U*-shape, respectively, and therefore, no NOE correlation of H_b-H_d should be present in conformation *U*. As shown in NOESY spectra performed in $CDCl_3$ at 313 K (Figure S6 and Figure 1d), the cross-correlation resonance peaks between the protons of T/Se and adjacent phenyl protons (H_c and H_d) were observed for two dimers, which can exclude the conformation *U*. Due to the poor solubility of DIBP3F-Se in $CDCl_3$ at 313 K, the NOESY signal is not clear enough, therefore, the high-temperature (333 K) 2D NOESY in CD_2Cl_4 was performed (Figure 1e), which show a good agreement with the spectrum in $CDCl_3$ at 313 K (Figure S6). The NOESY result implies that the dimers should exhibit either *S* or *O*-shaped conformation. However, the ^{19}F NMR spectra of both molecules (Figure S7) present only three distinct types of aromatic fluorine peaks, indicating that the OAs can only adopt *O*- or *U*-shape conformations (with four peaks corresponding to *S*-shape). Consequently, based on these spectral observations, it can be concluded that the dimeric acceptors can only adopt stable *O*-shaped conformation. It is noteworthy that our conclusion is not consistent with the general belief that hydrogen bonds are stronger than Van der Waals forces, where the strong F···H interactions should play a key role in the determination of the conformation and therefore, *U*-conformation should be preferred for the dimers. Surprisingly, our investigations revealed that the non-covalent intramolecular interactions (discuss below) in the conformation *O* were primarily characterized by weak F···S and F···Se interactions, rather than F···H interactions. Furthermore, it was notable to observe that both dimers exhibited relatively short calculated π–π stacking distances of 3.2 Å between their two end-groups in the *O*-shaped conformation, indicating strong intramolecular interactions between the two terminal IC moieties. This intriguing phenomenon can be attributed to the presence of a "conformational lock" resulting from the close proximity of the end-groups, ultimately leading to the adoption of the *O*-shaped conformation by the OAs.

Then, as presented in Table S3, the interatomic distances of F···S and F···Se for two acceptors based on *O*-shape were calculated to be 2.78 and 2.75 Å, respectively, which is shorter than the sum of the van der Waals radii of F–S (3.10 Å), F–Se (3.27 Å), indicating the existence of F···S and F···Se non-covalent intramolecular interactions in DIBP3F-S and DIBP3F-Se, respectively, and thus planar backbones can be expected.[17] As shown in Figure 1b–c, a dihedral angle of 6.2° was obtained between the linker and the adjacent BFIC-3F blocks in DIBP3F-Se, which is smaller than that of DIBP3F-S (10.6°) and facilitates the formation of better intermolecular stacking. Note that the dihedral angles of both dimeric acceptors are lower than those of the reported dimers and trimers without fluorine on the connected end groups.[9a–b,10]

Therefore, the molecular aggregation behavior of the two OAs in the solution phase was studied at different temperatures, and temperature-dependent optical absorption was recorded in a range of 20 to 60 °C in diluted chloroform solutions. As shown in Figure S8, as temperature increased, slightly blue shifts are found in the whole absorption range for both DIBP3F-S and DIBP3F-Se, clearly indicating a common heating-induced de-aggregating phenomenon and the existence of pre-aggregation of these OAs in their solution phase at lower temperatures. Figure S9 and Figure 2a present the UV/Vis absorption spectra of OAs in solution and thin film, respectively. Compared to their absorption in diluted chloroform solution, the spectra of DIBP3F-Se and DIBP3F-S in thin films exhibit significantly broader and red-shifted absorption (58 nm for DIBP3F-Se and 55 nm for DIBP3F-S in their λ_{max}, Table S4) with the identical absorption onset estimated at 904 nm, corresponding to an optical band gap (E_g) of 1.37 eV. Moreover, DIBP3F-Se shows enhanced vibrational shoulder peaks at 799 nm and a slightly higher absorption coefficient of $1.49\times10^5\ cm^{-1}$ than that of DIBP3F-S ($1.42\times10^5\ cm^{-1}$, Figure S10). The former indicates enhanced intermolecular π–π interactions and therefore more pronounced aggregation characteristics in thin films, which will be confirmed in the molecular packing analysis.

Grazing incidence wide-angle X-ray scattering (GIWAXS)[18] was performed to assess the molecular packing, structure ordering, and crystallinity of acceptors (Figure S11 and Table S5). Distinct (100) diffraction peaks in the in-plane (IP) direction and π–π stacking (010) ones in the out-of-plane (OOP) direction were observed for both acceptors, suggesting dominant face-on orientations relative to their substrates, which are often favorable for charge transport in a vertical direction in PSCs. A similar but slightly tighter π–π stacking diffraction was observed in DIBP3F-Se than in DIBP3F-S with a *d*-spacing of 3.75 Å for the former and 3.77 Å for the latter. However, compared with DIBP3F-S, DIBP3F-Se exhibits obviously reduced *d*-spacing (DIBP3F-Se = 15.87 Å at $q = 0.40\ Å^{-1}$; DIBP3F-S = 16.51 Å at $q = 0.38\ Å^{-1}$) and increased crystal coherence length (*CCL*, 65.07 Å for DIBP3F-Se; 58.12 Å for DIBP3F-S) along the IP direction, suggesting that the Se-based OA exhibits closer in plane molecular stacking and more ordered molecular packing in film than *S*-based one does. As a result, the electron mobility (μ_e) measured from the space-charge limited current (SCLC) method[19] increases from $7.77\times10^{-4}\ cm^2\,V^{-1}\,s^{-1}$ for DIBP3F-S to $8.95\times10^{-4}\ cm^2\,V^{-1}\,s^{-1}$ for DIBP3F-Se, which agrees well with their molecular packing characteristics.

These energy levels in films may be different due to the molecular-packing and -interactions. Cyclic voltammetry (CV) was performed to estimate their energy levels (Figure S12, Table S6). Both OAs exhibit very close HOMO/LUMO energy levels of −6.00/−4.27 eV for DIBP3F-Se and −6.03/−4.29 eV for DIBP3F-S (a difference of 0.03/0.02 eV) (Figure 2b). To confirm the small variation in LUMO energy levels, photoelectron spectroscopy in air (PESA) measurements were carried out.[20] The HOMO/LUMO energy levels of DIBP3F-Se and DIBP3F-S are calculated to be −5.67/−3.82 eV and −5.68/−3.85 eV, respectively (Figure S13), which are consistent with their CV results. The upshifted LUMO of DIBP3F-Se, as obtained from both CV and PESA measurements, could lead to a larger V_{oc} of PSCs when blending with the common PD PM6.

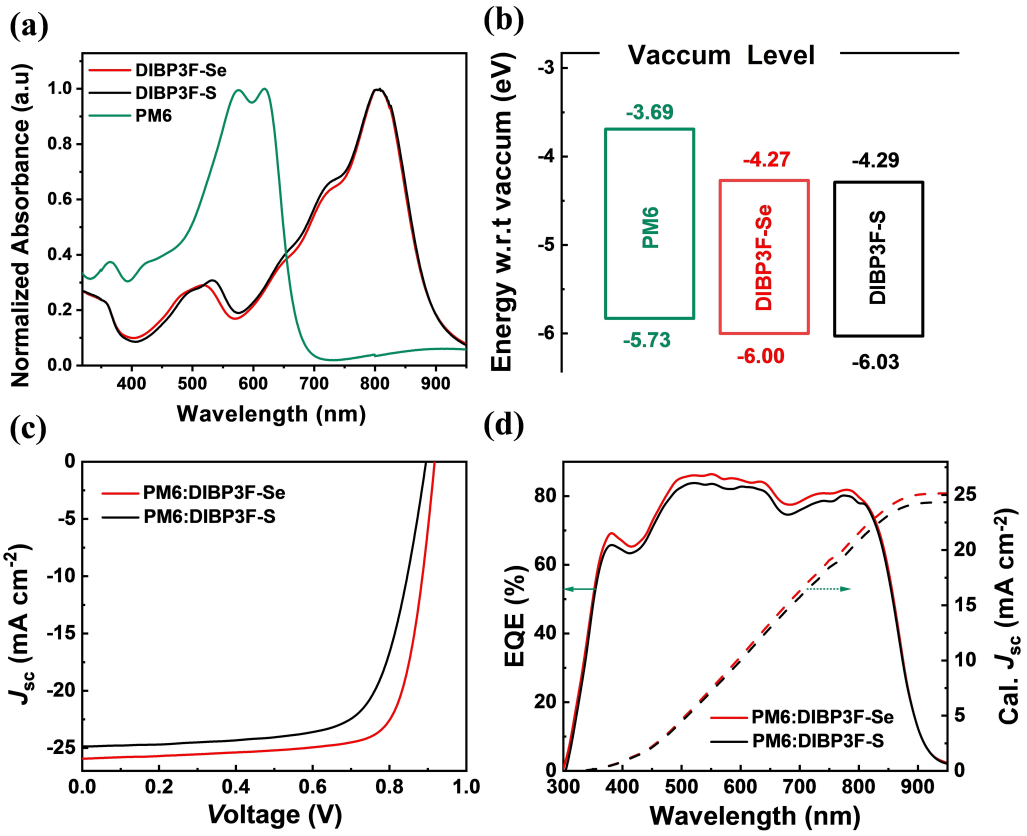

Figure 2. (a) Normalized UV–vis absorption spectra in pristine films and (b) energy levels of PM6, DIBP3F-Se, and DIBP3F-S. (c) *J*–*V* characteristics and (d) EQE curves and integrated J_{sc} values for optimized devices based on PM6 : DIBP3F-Se and PM6 : DIBP3F-S.

To investigate the impact of such different center π-bridge of these OAs as NFAs on their PV performance of PSCs, we fabricated solar cells using the conventional device architecture (SI). The device performance was optimized by varying the amount of solvent additive (1-chloronaphthalene) and thermal annealing conditions of the BHJ (Figure S14–15 and Table S7–8). Their current density-voltage (*J*–*V*) characteristics are illustrated in Figure 2c, and the corresponding PV parameters are summarized in Table 1. DIBP3F-S-based devices exhibit a PCE of 16.11 % with an open-circuit voltage (V_{oc}) of 0.901 V, a short-circuit current density (J_{sc}) of 24.86 mA cm^{-2}, and a fill factor (FF) of 72.0 %. Those based on DIBP3F-Se show enhanced V_{oc} of 0.917 V, a considerably improved J_{sc} of 25.92 mA cm^{-2} and a higher FF of 76.1 %, leading to a much higher PCE up to 18.09 %. The latter value is among the highest PCEs reported for OAs-based PSCs. Moreover, the PM6 : DIBP3F-Se cells exhibit a relatively lower E_{loss} ($E_{loss} = E_g^{PV} - qV_{oc}$, where E_g^{PV} is determined from the derivatives of the external quantum efficiency (EQE) curve,[21] shown in Figure S16) of ca. 0.509 eV, compared to that of PM6 : DIBP3F-S-based devices (0.527 eV). As discussed above, the upshifted LUMO and higher absorption coefficient of DIBP3F-Se should mainly account for the cell's higher V_{oc}, J_{sc}, and lower E_{loss}. Figure 2d displays the EQE curves of the DIBP3F-Se- and DIBP3F-S-based devices. Both PSCs show comparable photon-to-electron responses in the range of 350–900 nm with a maximum EQE of over 80 %. Moreover, the integrated J_{sc} values calculated from the corresponding EQE curves are 25.20 and 24.37 mA cm^{-2} for PM6 : DIBP3F-Se and PM6 : DIBP3F-S cells, respectively, with a less than 3 % mismatch as compared to the J_{sc} measured from *J*–*V* curves under simulated solar irradiation. Furthermore, to explore the compatibility of the OAs with other donors, the commonly used donor polymers D18 and PTQ-10 were selected to be paired with DIBP3F-Se (Figure S17 and Table S9). As demonstrated, the resulting DIBP3F-Se-based PSCs maintained an efficiency level of over 17 %.

Moreover, the device stability of the two OAs was also compared. Firstly, T_g was obtained by means of differential

Table 1: Photovoltaic performance of the PSCs based on PM6: acceptor (1 : 1, w/w) under the illumination of AM 1.5 G, 100 mW cm^{-2}.

D : A	V_{oc} [V]	J_{sc} [mA cm^{-2}]	Cal. J_{sc}[a] [mA cm^{-2}]	FF	PCE$_{max}$ [%]
PM6 : DIBP3F-Se	0.917	25.92	25.20	0.761	18.09 (17.86 ± 0.23)[b]
PM6 : DIBP3F-S	0.901	24.86	24.37	0.720	16.11

[a] The integral J_{sc} in brackets were calculated from the EQE curves. [b] The average PCE values were obtained from 20 devices and shown in brackets.

scanning calorimetry (DSC) scan, as shown in Figure S18, both OAs exhibit high T_g values above 180 °C, which can inhibit their diffusion in the polymer blends for de-mixing and maintain better device stability. DIBP3F-S exhibits a higher T_g of 199 °C than that of DIBP3F-Se (184 °C). Promisingly, the device based on DIBP3F-Se still presents better long-term stability than the DIBP3F-S-based one. As shown in Figure S19 after being tracked at the maximum power point tracking (MPPT) for 140 h, the Se-based cell could maintain higher initial efficiency than the devices based on PM6:DIBP3F-S. In addition, after being aged at 85 °C, it is obvious that the PM6:DIBP3F-Se-based OPV cell exhibits a larger T_{80} (more stable) of 22 days, followed by the PM6: DIBP3F-S-based cells with a T_{80} of 13 days. After being aged for 35 days, the PCEs for the PM6:DIBP3F-Se-based cell are also higher compared with the PM6:DIBP3F-S-based cells (Figure S20) which would be caused by the relatively stable morphology during the ageing process.

The miscibility between the donor and acceptor materials was studied using contact angle measurements. As shown in Table S10, the surface energy (γ)[22] was estimated to be 22.90, 28.82, and 30.56 mN m^{-1} for PM6, DIBP3F-Se, and DIBP3F-S, respectively. The compatibility between the different materials was then evaluated using the equation $\chi = K(\gamma_D^{-2} - \gamma_A^{-2})^2$, where χ is the Flory-Huggins interaction parameter, γ_D and γ_A are the γ of the donor PM6 and the OAs, respectively.[23] The PM6:DIBP3F-Se blend shows a lower χ value (0.340) than that of the PM6:DIBP3F-S blend (0.552), which indicates better miscibility of PM6 and DIBP3F-Se. Therefore, a slightly higher root mean square (RMS) surface roughness of 1.09 nm of the DIBP3F-S-based blend (0.91 nm for DIBP3F-Se) is shown in their atomic force microscopy (AFM) images in Figure 3b–e. The transmission electron microscopy (TEM) images of the DIBP3F-Se-based blend present a more desirable morphology with relatively smaller phase-separated domains compared to the DIBP3F-S, which facilitates efficient exciton dissociation

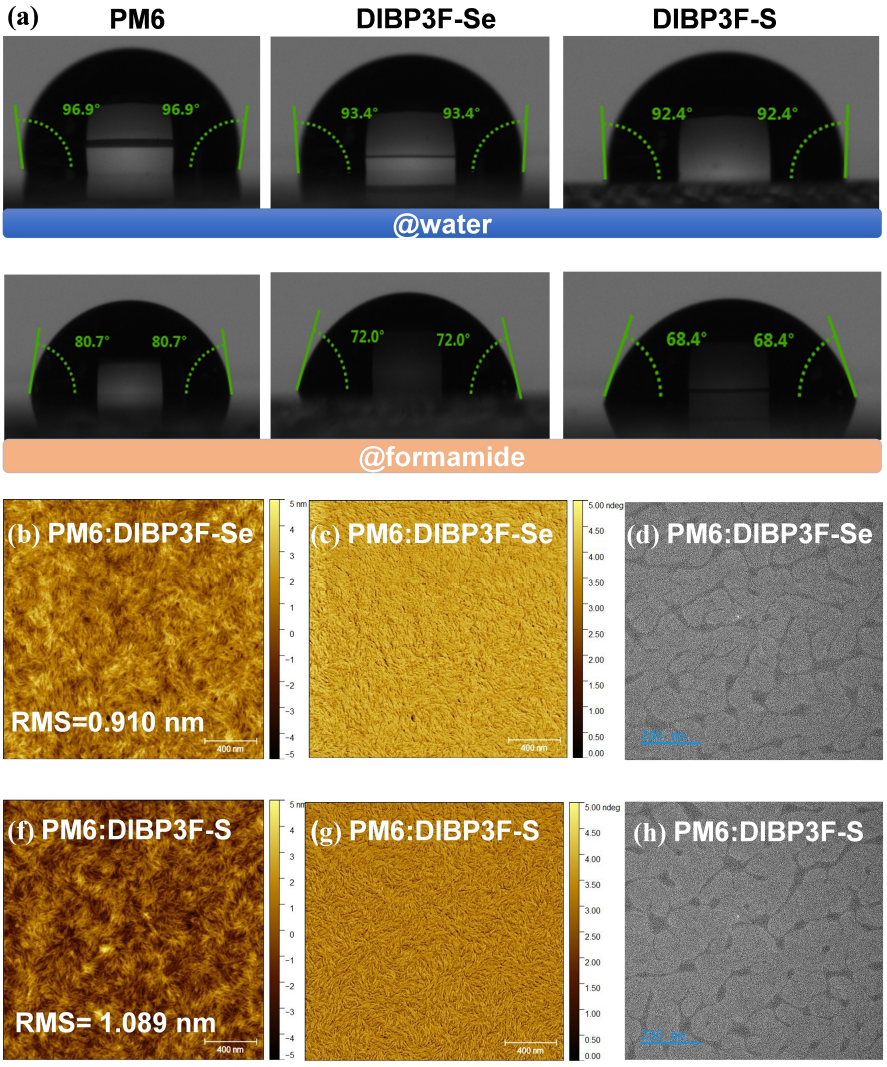

Figure 3. (a) The contact angle images of PM6, DIBP3F-Se, and DIBP3F-S films. (b, c) Tapping mode AFM topography height-, (d, e) phase-image, and (f, g) TEM images of PM6:DIBP3F-Se, PM6:DIBP3F-S blend films.

and charge transport, and suppresses charge recombination, thus leading to such enhanced J_{sc} and FF as being measured.

For the molecular orientation and crystalline properties of the blend films (PM6:DIBP3F-S and PM6:DIBP3F-Se), both blend films exhibit a predominant face-on molecular arrangement by following the same trend of the neat films from OAs (Figure 4) and PM6 (Figure S21). Both blend films present similar *CCL* values (DIBP3F-Se = 24.88 Å; DIBP3F-S = 24.39 Å) in the OOP direction. The packing distance calculated from (100) peak in the IP direction can be assigned to the donor polymer PM6 as the peak positions are similar in both neat and blend films of PM6 at ~0.30 $Å^{-1}$. Compared with PM6:DIBP3F-S, the PM6:DIBP3F-Se blend exhibits a similar *d*-spacing (20.98 Å for DIBP3F-Se; 20.69 Å for DIBP3F-S) but a significantly enhanced *CCL* (111.23 Å for DIBP3F-Se; 93.56 Å for DIBP3F-S) in the IP direction, implying its stronger crystallization propensity. It is such improved molecular packing and crystallinity of the blend film that well explains the enhanced J_{sc} and FF of the relative PSCs with effective exciton dissociation and fewer recombination losses. In summary, the data and analysis presented so far demonstrate that the incorporation of selenophene spacer in the dimeric-type acceptors can prompt better molecular packing, improved morphology of the blends,[24] enhanced charge-separation and -transport in active layers, and thereby the overall performance of the PSCs.

The hole- (μ_h) and electron-mobilities of the two blends were measured by using the SCLC[20] technique (Figure 5a and Figure S22), which indicates that the PM6:DIBP3F-Se blend presents higher μ_h and μ_e mobilities and a more balanced μ_h/μ_e ratio as compared to PM6:DIBP3F-S. This is mostly attributed to the improved film morphology (e.g. smoother and more compact) and the presence of its smaller phase-separated domains. Moreover, the carrier mobility (μ) determined by photoinduced charge-carrier extraction in linearly increasing voltage (photo-CELIV) measurement (Figure 5a and Figure S23) in the PM6:DIBP3F-Se-based device ($7.28\times10^{-4}\ cm^2V^{-1}s^{-1}$) is higher than that of the PM6:DIBP3F-S-based one ($6.24\times10^{-4}\ cm^2V^{-1}s^{-1}$), which is consistent with the SCLC measurements.

Next, the kinetics of charge recombination in both devices were studied. We performed light intensity (P_{light}) transient photovoltage (TPV) and charge-extraction (CE) measurements (Figure 5b and Figure S24).[26] The carrier lifetimes (τ) of 11.2 μs for the DIBP3F-Se-based device is much longer than that based on DIBP3F-S (7.21 μs), indicating a lower carrier recombination rate for the case of the PM6:DIBP3F-Se BHJ. Moreover, the τ for the DIBP3F-Se-based device is higher than that of the DIBP3F-S-based one at various carrier density (n) with a lower recombination order (λ) of 1.54. Based on these results, the bimolecular recombination rate constants (k_{rec}) were obtained using $k_{rec} = 1/[(\lambda+1)]\ nr$.[26] Evidently, the k_{rec} for the device based on DIBP3F-Se is lower than that for the DIBP3F-S blend (Figure 5c), which explains suppressed charge recombination and improves the overall performance of the cells.

To gain further insights into the charge generation and exciton dissociation in the devices comprising different acceptors, we plot the photocurrent density (J_{ph}) with respect to the effective voltage (V_{eff})[27] (Figure 5d). The DIBP3F-Se-based device has larger J_{ph}/J_{sat} of 98.0 % under short-circuit condition and 95.4 % under the maximal power

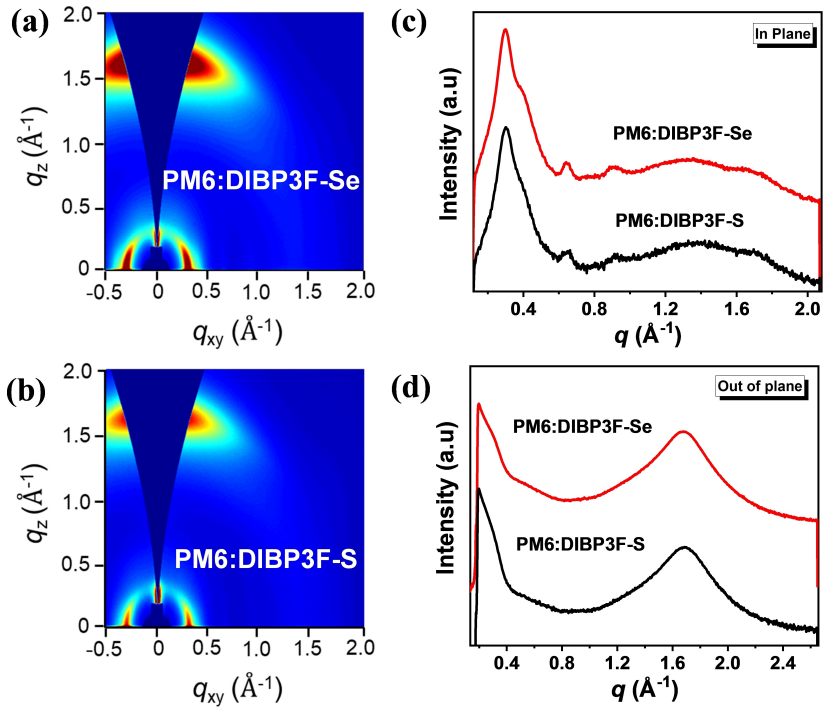

Figure 4. 2D GIWAXS profiles (a, b) and the corresponding 1D line cuts (c, d) of PM6:DIBP3F-Se and PM6:DIBP3F-S blend films.

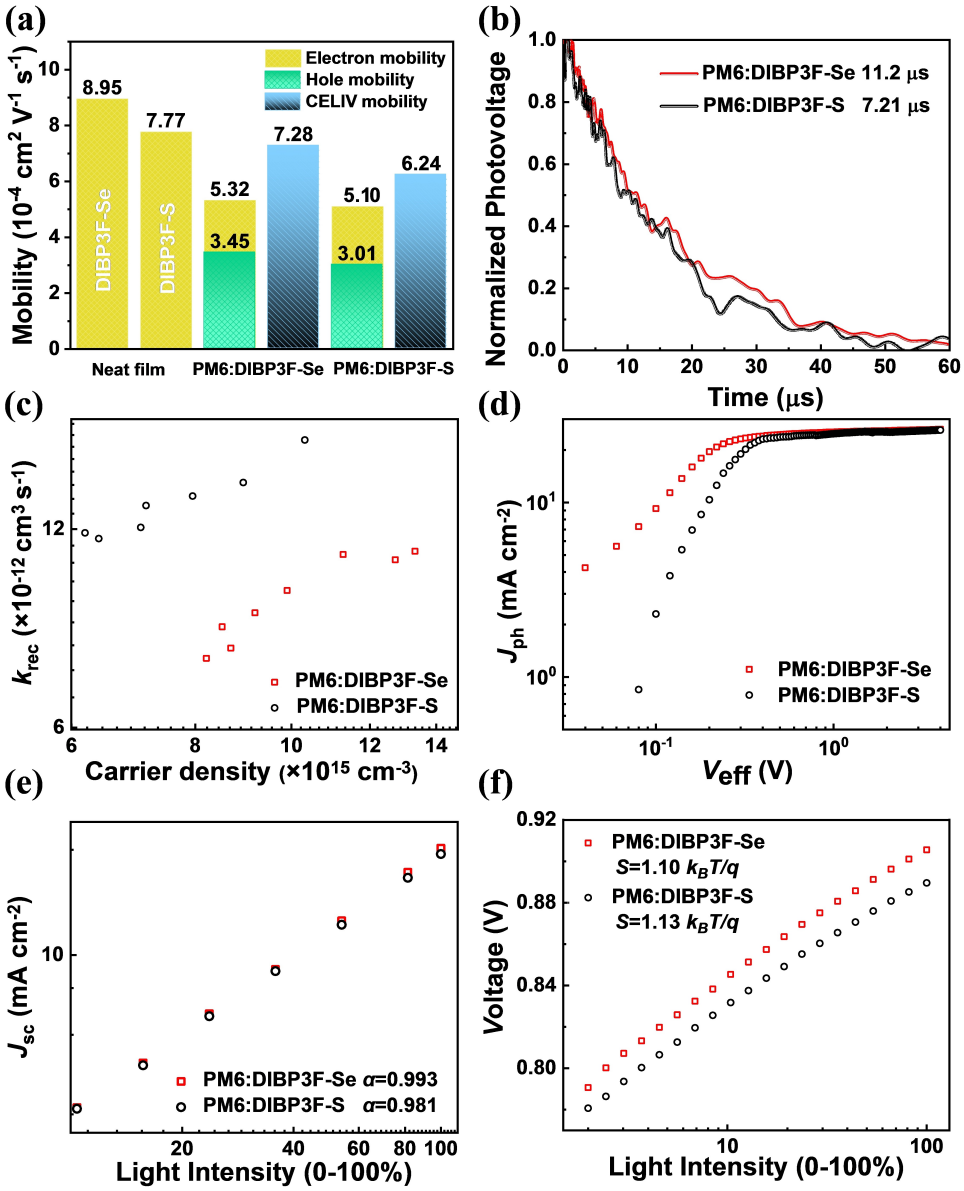

Figure 5. (a) Hole- and electron-mobilities of the devices and CELIV mobilities. (b) Normalized TPV data for the investigated PM6-based devices. (c) The k_{rec} inferred from τ and n, as a function of n. (d) Characteristics of J_{ph} versus V_{eff}. Light intensity dependence on (e) J_{sc} and (f) V_{oc} for the optimized PSCs.

output condition than that of the DIBP3F-S-based cell (96.4 % and 94.9 %, respectively), indicating more efficient charge carrier dissociation in PM6:DIBP3F-Se BHJ. Moreover, the dependencies of J_{sc} (Figure 5e) and V_{oc} (Figure 5f) on P_{light}, were measured in order to further study the charge recombination mechanism. The relationship between J_{sc} and P_{light} can be defined as $J_{sc} \propto (P_{light})^{\alpha}$, where an α value close to 1 suggests weak bimolecular recombination.[28] The DIBP3F-Se-based PSC yields an α value closer to 1 ($\approx$0.993) as compared to DIBP3F-S-based cells ($\approx$0.981). Moreover, the slope of V_{oc} versus lg(P_{light}) is used to estimate the degree of trap-assisted recombination.[29] Cells based on DIBP3F-Se show a smaller slope of 1.10 k_BT/q (where k is the Boltzmann constant, T is the absolute temperature (in K) and q is the elementary charge) than that of DIBP3F-S (1.13 k_BT/q), revealing that the Se-substituted acceptor has fewer the trap-assisted recombination or geminate recombination. As a result, the PM6:DIBP3F-Se-based PSC exhibit enhanced exciton dissociation and charge collection, which explains the boost in both J_{sc} and FF.

Conclusion

In conclusion, two new dimeric-type acceptors, DIBP3F-Se and DIBP3F-S, were synthesized by bridging Y6-derivative with selenophene and thiophene linkage units, respectively, and tested with the state-of-the-art polymer donor PM6 in PSCs. Unlike "routinely recognized" in previous reports, which suggest that strong hydrogen bonding, such as H···F

and H···O, should serve as a "conformational lock" in the determination of molecular conformation (*U*-conformation should be preferable by following this suggestion), our findings propose a different scenario. Through NMR experimental measurements and DFT simulations, we have demonstrated that both acceptors adopt an *O*-shaped conformations, induced by a unique "conformational lock" resulting from the robust intramolecular π–π interaction between their two terminal IC groups. Additionally, DIBP3F-Se exhibits a higher absorption coefficient, up-shifted LUMO energy level, higher backbone co-planarity, and more ordered molecular packing in the solid state than that of DIBP3F-S, which leads to overall improved photoelectric performance. When blended with PM6, morphological and device studies revealed that the PM6:DIBP3F-Se system exhibited better phase segregation with improved molecular packing and crystallinity. These characteristics led to superior charge photogeneration, enhanced carrier transport, and suppressed charge recombination with decreased energy loss ultimately yielding solar cells with a PCE value of 18.09 %, which is one of the highest values reported to date for oligomeric acceptor-based PSCs. Moreover, DIBP3F-Se also presents a good compatibility as an acceptor when being paired with D18 and PTQ-10 as the donor, resulting in PCE of over 17 % in PSCs, respectively. These encouraging results close the gap between the PCEs of oligomeric acceptor-based devices and those of conventional SMA-based ones, demonstrating the promise of dimeric-type acceptors for high-performance PSCs. Our study provides useful insights into the determination of the conformation of OAs and design guidelines for the development of dimeric acceptors for future high-performance PSCs.

Acknowledgements

We thank the Swedish Research Council (2016-06146, 2019-04683, 2020-05233), Swedish Research Council Formas, Knut and Alice Wallenberg Foundation (2017.0186, 2016.0059), Swedish Energy Agency (Grant number: P2021-90067), STINT and STandUP for Energy collaboration. Computations/simulations were performed at Chalmers e-Commons (C3SE) and Swedish National Infrastructure for Computing (SNIC) at the National Supercomputer Centre (NSC) at Linköping University. J. W. acknowledges the support from the Chinese Scholarship Council. T.D.A., Z.H., C. C., X.C., F.H.I., F.L., acknowledge support by the KAUST Office of Sponsored Research (OSR) under Awards No: OSR-2018-CARF/CCF-3079 and No: OSR-2019-CRG8-4095.3. H.Y.W. acknowledges the support from the National Research Foundation of Korea (2019R1A6A1A11044070). Support from Sino-Danish Center (SDC) for Education and Research is fully acknowledged. The 2D NMR measurements were performed at the Swedish NMR Center, in Gothenburg, Sweden. Grateful for the discussion with Prof. Reinhard Wimmer from Aalborg University on a conformational determination.

Conflict of Interest

The authors declare no conflict of interest.

Data Availability Statement

The data that support the findings of this study are available from the corresponding author upon reasonable request.

Keywords: Acceptor · Molecular Conformation · Oligomer · Selenophene · Solar Cells

[1] a) P. Cheng, G. Li, X. Zhan, Y. Yang, *Nat. Photonics* **2018**, *12*, 131–142; b) J. Hou, O. Inganas, R. H. Friend, F. Gao, *Nat. Mater.* **2018**, *17*, 119–128.

[2] a) H. Chen, S. Y. Jeong, J. Tian, Y. Zhang, D. R. Naphade, M. Alsufyani, W. Zhang, S. Griggs, H. Hu, S. Barlow, H. Y. Woo, S. R. Marder, T. D. Anthopoulos, I. McCullochbd, Y. Lin, *Energy Environ. Sci.* **2023**, *16*, 1062–1070; b) W. Gao, F. Qi, Z. Peng, F. R. Lin, K. Jiang, C. Zhong, W. Kaminsky, Z. Guan, C. S. Lee, T. J. Marks, H. Ade, A. K. Jen, *Adv. Mater.* **2022**, *34*, 2202089; c) A. Karki, A. J. Gillett, R. H. Friend, T. Q. Nguyen, *Adv. Energy Mater.* **2021**, *11*, 2003441 ; d) Y. Lin, Y. Zhang, A. Magomedov, E. Gkogkosi, J. Zhang, X. Zheng, A. El-Labban, S. Barlow, V. Getautis, E. Wang, L. Tsetseris, S. R. Marder, I. McCullochb, T. D. Anthopoulos, *Mater. Horiz.* **2023**, *10*, 1292–1300.

[3] a) J. Wang, Y. Cui, Y. Xu, K. Xian, P. Bi, Z. Chen, K. Zhou, L. Ma, T. Zhang, Y. Yang, Y. Zu, H. Yao, X. Hao, L. Ye, J. Hou, *Adv. Mater.* **2022**, *34*, 2205009; b) H. Yu, Y. Wang, H. K. Kim, X. Wu, Y. Li, Z. Yao, M. Pan, X. Zou, J. Zhang, S. Chen, D. Zhao, F. Huang, X. Lu, Z. Zhu, H. Yan, *Adv. Mater.* **2022**, *34*, 2200361.

[4] a) Y. Lin, J. Wang, Z. G. Zhang, H. Bai, Y. Li, D. Zhu, X. Zhan, *Adv. Mater.* **2015**, *27*, 1170–1174; b) Q. Wei, W. Liu, M. Leclerc, J. Yuan, H. Chen, Y. Zou, *Sci. China Chem.* **2020**, *63*, 1352–1366; c) J. Wu, G. Li, J. Fang, X. Guo, L. Zhu, B. Guo, Y. Wang, G. Zhang, L. Arunagiri, F. Liu, H. Yan, M. Zhang, Y. Li, *Nat. Commun.* **2020**, *11*, 4612.

[5] a) M. Ghasemi, H. Hu, Z. Peng, J. J. Rech, I. Angunawela, J. H. Carpenter, S. J. Stuard, A. Wadsworth, I. McCulloch, W. You, H. Ade, *Joule* **2019**, *3*, 1328–1348; b) H. Hu, M. Ghasemi, Z. Peng, J. Zhang, J. J. Rech, W. You, H. Yan, H. Ade, *Adv. Mater.* **2020**, *32*, 2005348.

[6] a) Q. Chen, Y. H. Han, L. R. Franco, C. F. N. Marchiori, Z. Genene, C. M. Araujo, J. W. Lee, T. N. Phan, J. Wu, D. Yu, D. J. Kim, T. S. Kim, L. Hou, B. J. Kim, E. Wang, *Nano-Micro Lett.* **2022**, *14*, 164; b) Z. Genene, J. W. Lee, S. W. Lee, Q. Chen, Z. Tan, B. A. Abdulahi, D. Yu, T. S. Kim, B. J. Kim, E. Wang, *Adv. Mater.* **2022**, *34*, 2107361; c) Q. Wu, W. Wang, Y. Wu, R. Sun, J. Guo, M. Shi, J. Min, *Natl. Sci. Rev.* **2022**, *9*, nwab151; d) Z. G. Zhang, Y. Li, *Angew. Chem. Int. Ed. Engl.* **2021**, *60*, 4422–4433.

[7] a) J. Jia, Q. Huang, T. Jia, K. Zhang, J. Zhang, J. Miao, F. Huang, C. Yang, *Adv. Energy Mater.* **2022**, *12*, 2103193; b) H. K. H. Lee, Z. Li, I. Constantinou, F. So, S. W. Tsang, S. K. So, *Adv. Energy Mater.* **2014**, *4*, 1400768; c) W. Wang, Q. Wu, R. Sun, J. Guo, Y. Wu, M. Shi, W. Yang, H. Li, J. Min, *Joule* **2020**, *4*, 1070–1086; d) H. Yang, C. Cui, *Energy Rev.* **2022**, *1*, 100008.

[8] T. Jia, J. Zhang, W. Zhong, Y. Liang, K. Zhang, S. Dong, L. Ying, F. Liu, X. Wang, F. Huang, Y. Cao, *Nano Energy* **2020**, *72*, 104718.

[9] a) H. Wang, C. Cao, H. Chen, H. Lai, C. Ke, Y. Zhu, H. Li, F. He, *Angew. Chem. Int. Ed. Engl.* **2022**, *61*, e202201844; b) Y. Liang, D. Zhang, Z. Wu, T. Jia, L. Lüer, H. Tang, L. Hong, J. Zhang, K. Zhang, C. J. Brabec, N. Li, F. Huang, *Nat. Energy* **2022**, *7*, 1180–1190; c) L. Zhang, Z. Zhang, D. Deng, H. Zhou, J. Zhang, Z. Wei, *Adv. Sci.* **2022**, *9*, e2202513; d) C. Sun, J. W. Lee, C. Lee, D. Lee, S. Cho, S. K. Kwon, B. J. Kim, Y. H. Kim, *Joule* **2023**, *7*, 416–430; e) J.-W. Lee, C. Sun, C. Lee, Z. Tan, T. N. Phan, H. Jeon, D. Jeong, S. Kwon, Y. Kim, B. J. Kim, *ACS Energy Lett.* **2023**, *8*, 1344–1353.

[10] W. Liu, J. Yuan, C. Zhu, Q. Wei, S. Liang, H. Zhang, G. Zheng, Y. Hu, L. Meng, F. Gao, Y. Li, Y. Zou, *Sci. China Chem.* **2022**, *65*, 1374–1382.

[11] Q. Shen, C. He, S. Li, L. Zuo, M. Shi, H. Chen, *Acc. Mater. Res.* **2022**, *3*, 644–657.

[12] a) H. Huang, L. Yang, A. Facchetti, T. J. Marks, *Chem. Rev.* **2017**, *117*, 10291–10318; b) Y. Liu, Z. Zhang, S. Feng, M. Li, L. Wu, R. Hou, X. Xu, X. Chen, Z. Bo, *J. Am. Chem. Soc.* **2017**, *139*, 3356–3359.

[13] X. Gu, Y. Wei, N. Yu, J. Qiao, Z. Han, Q. Lin, X. Han, J. Gao, C. Li, J. Zhang, X. Hao, Z. We, Z. Tang, Y. Cai, X. Zhang, H. Huang, *CCS Chem.* **2023**, https://doi.org/10.31635/ccschem.023.202202575.

[14] a) A. M. da Silva, A. Ghosh, P. Chaudhuri, *J. Phys. Chem. A* **2013**, *117*, 10274–10285; b) L. R. Franco, K. C. F. Toledo, T. A. Matias, P. A. Benavides, H. M. Cezar, C. M. Araujo, K. Coutinho, K. Araki, *Phys. Chem. Chem. Phys.* **2022**, *24*, 10222–10240.

[15] H.-Y. Chen, S.-C. Yeh, C.-T. Chen, C.-T. Chen, *J. Mater. Chem.* **2012**, *22*, 21549.

[16] M. Chatzopoulou, R. F. Martínez, N. J. Willis, T. D. W. Claridge, F. X. Wilson, G. M. Wynne, S. G. Davies, A. J. Russell, *Tetrahedron* **2018**, *74*, 5280–5288.

[17] W. Gao, H. Fu, Y. Li, F. Lin, R. Sun, Z. Wu, X. Wu, C. Zhong, J. Min, J. Luo, H. Y. Woo, Z. Zhu, A. K. Y. Jen, *Adv. Energy Mater.* **2021**, *11*, 2003177.

[18] a) E. Gann, A. T. Young, B. A. Collins, H. Yan, J. Nasiatka, H. A. Padmore, H. Ade, A. Hexemer, C. Wang, *Rev. Sci. Instrum.* **2012**, *83*, 045110; b) P. Müller-Buschbaum, *Adv. Mater.* **2014**, *26*, 7692–7709; c) D. Yuk, M. H. Jee, C. W. Koh, W. W. Park, H. S. Ryu, D. Lee, S. Cho, S. Rasool, S. Park, O. H. Kwon, J. Y. Kim, H. Y. Woo, *Small* **2023**, *19*, e2206547.

[19] C. M. Proctor, C. Kim, D. Neher, T.-Q. Nguyen, *Adv. Funct. Mater.* **2013**, *23*, 3584–3594.

[20] K. Yoshino, M. Onoda, Y. Manda, M. Yokoyama, *Jpn. J. Appl. Phys.* **1988**, *27*, L1606.

[21] Y. Wang, D. Qian, Y. Cui, H. Zhang, J. Hou, K. Vandewal, T. Kirchartz, F. Gao, *Adv. Energy Mater.* **2018**, *8*, 1801352.

[22] D. K. Owens, R. C. Wendt, *J. Appl. Polym. Sci.* **1969**, *13*, 1741–1747.

[23] H. Xia, Y. Zhang, W. Deng, K. Liu, X. Xia, C. J. Su, U. S. Jeng, M. Zhang, J. Huang, J. Huang, C. Yan, W. Y. Wong, X. Lu, W. Zhu, G. Li, *Adv. Mater.* **2022**, *34*, e2107659.

[24] M. Privado, A. Agrawal, P. de la Cruz, M. L. Keshtov, G. D. Sharma, F. Langa, *Solar RRL* **2022**, *6*, 2100768.

[25] A. Pivrikas, N. S. Sariciftci, G. Juška, R. Österbacka, *Prog. Photovolt. Res. Appl.* **2007**, *15*, 677–696.

[26] Y. Lin, M. I. Nugraha, Y. Firdaus, A. D. Scaccabarozzi, F. Aniés, A.-H. Emwas, E. Yengel, X. Zheng, J. Liu, W. Wahyudi, E. Yarali, H. Faber, O. M. Bakr, L. Tsetseris, M. Heeney, T. D. Anthopoulos, *ACS Energy Lett.* **2020**, *5*, 3663–3671.

[27] J. L. Wu, F. C. Chen, Y. S. Hsiao, F. C. Chien, P. Chen, C. H. Kuo, M. H. Huang, C. S. Hsu, *ACS Nano* **2011**, *5*, 959–967.

[28] M. Lenes, M. Morana, C. J. Brabec, P. W. M. Blom, *Adv. Funct. Mater.* **2009**, *19*, 1106–1111.

[29] L. J. A. Koster, V. D. Mihailetchi, R. Ramaker, P. W. M. Blom, *Appl. Phys. Lett.* **2005**, *86*, 123509.

Manuscript received: February 25, 2023
Accepted manuscript online: June 28, 2023
Version of record online: ■■, ■■

Research Articles

Solar Cells

J. Wu, Z. Ling, L. R. Franco, S. Y. Jeong, Z. Genene, J. Mena, S. Chen, C. Chen, C. M. Araujo, C. F. N. Marchiori, J. Kimpel, X. Chang, F. H. Isikgor, Q. Chen, H. Faber, Y. Han, F. Laquai, M. Zhang, H. Y. Woo, D. Yu,* T. D. Anthopoulos,* E. Wang* — **e202302888**

On the Conformation of Dimeric Acceptors and Their Polymer Solar Cells with Efficiency over 18%

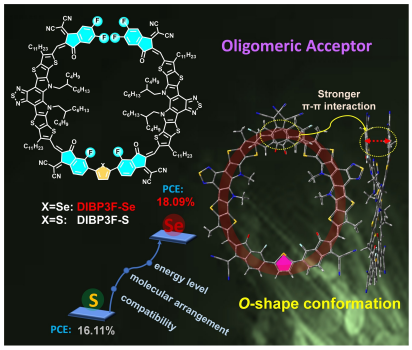

Two dimeric-type acceptors, DIBP3F-Se and DIBP3F-S were synthesized with selenophone and thiophene as a bridge, respectively. Both exhibit O-shape conformation as determined by NMR and DFT simulations, which is driven by the robust π–π interaction of intramolecular terminal groups. The PM6:DIBP3F-Se-based solar cell demonstrated an efficiency of 18.09%.